Atmos. Chem. Phys., 8, 6979–6993, 2008
www.atmos-chem-phys.net/8/6979/2008/

Atmospheric Chemistry and Physics

Observations of mesoscale and boundary-layer scale circulations affecting dust transport and uplift over the Sahara

J. H. Marsham[1], **D. J. Parker**[1], **C. M. Grams**[2], **B. T. Johnson**[4], **W. M. F. Grey**[3], **and A. N. Ross**[1]

[1]University of Leeds, UK
[2]Universität Karlsruhe and Forschungszentrum Karlsruhe, Germany
[3]Climate and Land Surface Systems Interaction Centre, School of the Environment and Society, Swansea, SA2 8PP, UK
[4]The Met Office, UK

Received: 16 November 2007 – Published in Atmos. Chem. Phys. Discuss.: 19 May 2008
Revised: 8 September 2008 – Accepted: 22 October 2008 – Published: 4 December 2008

Abstract. Observations of the Saharan boundary layer, made during the GERBILS field campaign, show that mesoscale land surface temperature variations (which were related to albedo variations) induced mesoscale circulations. With weak winds along the aircraft track, land surface temperature anomalies with scales of greater than 10 km are shown to significantly affect boundary-layer temperatures and winds. Such anomalies are expected to affect the vertical mixing of the dusty and weakly stratified Saharan Residual Layer (SRL). Mesoscale variations in winds are also shown to affect dust loadings in the boundary layer.

Using the aircraft observations and data from the COSMO model, a region of local dust uplift, with strong along-track winds, was identified in one low-level flight. Large eddy model (LEM) simulations based on this location showed linearly organised boundary-layer convection. Calculating dust uplift rates from the LEM wind field showed that the boundary-layer convection increased uplift by approximately 30%, compared with the uplift rate calculated neglecting the convection. The modelled effects of boundary-layer convection on uplift are shown to be larger when the boundary-layer wind is decreased, and most significant when the mean wind is below the threshold for dust uplift and the boundary-layer convection leads to uplift which would not otherwise occur.

Both the coupling of albedo features to the atmosphere on the mesoscale, and the enhancement of dust uplift by boundary-layer convection are unrepresented in many climate models, but may have significant impacts on the vertical transport and uplift of desert dust. Mesoscale effects in particular tend to be difficult to parametrise.

Correspondence to: J. H. Marsham
(jmarsham@env.leeds.ac.uk)

1 Introduction

Mineral dust uplifted from deserts is an important component of Earth's climate system. The dust has a direct effect on the radiation budget (e.g. Haywood et al. 2005), and this affects atmospheric dynamics (Tompkins et al., 2005; Jones et al., 2004; Perez et al., 2006). Dust provides nuclei for ice formation in clouds (Field et al., 2006), can affect cloud organisation (Stephens et al., 2004), and provides iron essential for phytoplankton (Mahowald et al., 2005). Efforts to model the transport of desert dust in regional and global models are, however, still in their infancy (Woodward, 2001; Cakmur et al., 2006; Mahowald et al., 2006; Zakey et al., 2006).

The Sahara desert is the largest source of mineral dust in the atmosphere (approximately 60%, Tanaka and Chiba 2006), but is a very poorly observed region. Over the Sahara, large surface sensible heat fluxes and deep dry convection can result in a summertime boundary layer that is up to 6 km deep (Gammo, 1996). However, profiles from the Sahara in summer typically show a shallower active convective boundary layer (CBL), with a near neutrally stratified residual layer above (the Saharan Residual Layer, SRL). This is typically capped by a strong inversion at approximately 5.5 km. Where a colder boundary layer (e.g. from the monsoon or the ocean) has undercut the Saharan boundary layer,

Published by Copernicus Publications on behalf of the European Geosciences Union.

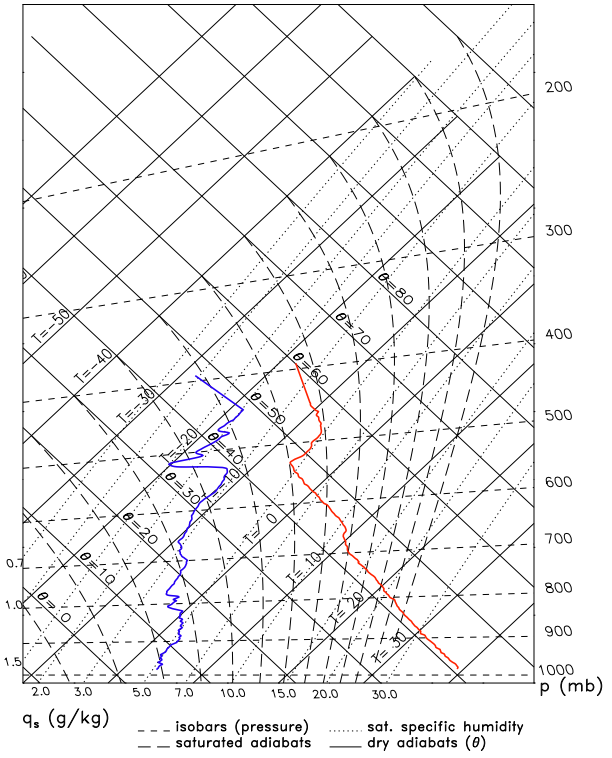

Fig. 1. Tephigram plot of a dropsonde profile from the Sahara (18° N, 8.25° W) taken during the GERBILS field campaign (12:39 UTC on the 24th June 2007).

the resultant elevated dry layer is referred to as the Saharan Air Layer (SAL). The deep dry SAL layer allows much of the Saharan dust plume to avoid rain-out over the Atlantic, allowing the dust to be transported globally. Furthermore, it has also often been observed that the SAL and SRL can contain distinct sub-layers, each with different water vapour and dust contents (Parker et al., 2005).

Figure 1 shows an example of the stratification of the SRL. The profile shows five distinct layers below the lid at 520 hPa, each essentially internally well mixed with a different water vapour mixing ratio (WVMR). Layers are separated by inversions, many of which are very weak (less than 1 K), and the strongest of which is 3 K (at $\simeq$650 hPa). This weak stratification of the SRL, and the weak lid between the convective boundary layer and the SRL, means that even small anomalies in the surface heating may significantly affect the growth of the CBL into the SRL. We expect land surface variations in desert regions to affect surface fluxes and so induce mesoscale circulations (Segal and Arritt, 1992). In particular, low albedo regions are expected to increase surface fluxes. As a result, low albedo regions are expected to locally increase the rate of growth of the CBL into the SRL, and so affect the vertical transport of dust between the CBL and SRL. In addition, mesoscale circulations generated by such land surface variations may also affect low-level winds and so the uplift of desert dust.

Observations of convective plumes and vortices from Arizona, USA (Koch and Renno, 2005) and large eddy modelling of the Gobi desert (Takemi et al., 2006) suggest that boundary-layer convection uplifts significant quantities of desert dust. Washington et al. (2006) also showed that during the morning in the Bodele depression boundary-layer convection mixes momentum from the nocturnal jet downwards, which results in dust uplift, and Cakmur et al. (2004) showed that allowing the sub-grid fluctuations in the boundary layer implicit in a global model to affect dust uplift improved the modelled dust distribution. Using Meteosat Second Generation observations Chaboureau et al. (2007) observed a diurnal cycle in the 10.8 minus 12 μm difference over West Africa, with its peak at 15:00 UTC, which they linked to boundary-layer activity. These results all show that small scale variations in low-level windspeeds are important for dust uplift and transport. However, such mesoscale and boundary-layer processes are not resolved, and often not represented, in climate models. In addition, there are very few published observations of these processes, and perhaps none for the western Sahara.

The GERBILS (GERB Intercomparison of Longwave and Shortwave radiation) field campaign, which took place in June 2007, aimed to understand the differences between modelled and observed outgoing radiative fluxes in the western Sahara (Haywood et al., 2005). Seven flights took place between Niamey (Niger) and Nouakchott (Mauritania), providing significant amounts of data, from this poorly observed region. Stratifications in dust loadings in the SRL and SAL (similar to the stratification in WVMR shown in Fig. 1) were often observed during the campaign (e.g. Fig. 5, and also Fig. 3 in Marsham et al., 2008), as has previously been observed (Parker et al., 2005).

Two flights from GERBILS provided long legs within the Saharan boundary layer; these were on the 27th and 28th June 2007 (B301 and B302). The objective of this paper is to show the impacts of land surface variations on the boundary layer which were observed during these flights. A large eddy model (LEM) simulation, based on an observed region of dust uplift, is then used to investigate the expected impacts of boundary-layer convection on dust uplift rates. Section 2 describes the data, models and methods used and Sects. 3.1 and 3.2 describe the observations from B302 and B301 respectively.

2 Data, model and methods used

2.1 Observations

A large array of instruments was present on the FAAM BAe146 aircraft during GERBILS and all data presented were recorded at 32 Hz, but one-second data was used for all

the analysis presented. This, and the response time of the instruments, were sufficient for the spatial scales considered in this paper (>200 m for winds, temperatures and humidities, and >5 km for other variables). In addition to standard meteorological parameters of temperature, humidity and winds, this paper makes use of measurements of: (i) downwelling and upwelling solar radiation (allowing solar albedo to be calculated), (ii) nephelometer scattering, and (iii) upwelling infrared radiation measured using a broadband Heimann radiometer. Nephelometer scattering was dominated by dust, and was observed at red, green and blue wavelengths. In this paper the nephelometer data are used as an indicator of dust loadings, and only blue data are shown, since differences between the three channels were small. The nephelometer measures aerosol scattering coefficient, i.e. the scattering cross-sectional area of the aerosols per unit volume of air.

All the Heimann radiometer data discussed in this paper were from low-level flights at constant altitudes, where variations in atmospheric absorption are expected to have small effects, and be slowly varying. The dust below the aircraft is expected to affect brightness temperatures (BTs) from the Heimann radiometer by less than 0.2 K, and again be quite smoothly varying[1]. The remaining variations in BTs from the Heimann radiometer are from variations in land surface temperatures (LSTs) and emissivities. Heimann BTs were significantly anticorrelated with albedo (Sect. 3.1). This shows that a significant component of the BT signal is from variability in LSTs (since in the cloud-free conditions discussed darker surfaces are expected to lead to increased LSTs). Furthermore, in this paper boundary-layer virtual potential temperatures are shown to be coherently related to Heimann BTs. Any variations in land emissivity will have tended to mask rather than generate this coherency, so in such cases the Heimann BTs are assumed to relate to LSTs.

Low-level legs during GERBILS were flown at constant pressure levels. The low level leg from B302 was at 640 to 710 m above mean sea level (MSL), or 290 to 470 m above the ground level (a.g.l.). This was in the lower CBL, at an a.g.l. height of approximately 0.18 to 0.35 times the CBL depth (see Sect. 3.1). The low level leg from B301 was higher, at approximately 950 m above m.s.l. (550 to 730 m a.g.l.). This was in the middle or upper CBL (see Sect. 3.3).

2.2 The COSMO and LEM models

Version 3.19 of the COSMO (Consortium for Small-scale Modeling) model (Doms and Schättler, 2002), from the Deutscher Wetterdienst (DWD), was run over a domain extending from 17° W to 2° E and 13° N to 23° N. COSMO is a non-hydrostatic model, and the model equations for fully compressible flow in a moist atmosphere are formulated in rotated geographical coordinates and a generalised terrain following height coordinate. The horizontal grid-spacing was 0.0625° (approximately 7 km) and 35 levels were used in the vertical (grid-spacing of approximately 10 m at the lowest model levels). Land use data, from DWD, were on the same 0.0625° grid as the model.

The model was initialised using operational analyses from the ECMWF (European Centre for Medium Range Weather Forecasts) global model, which has a 0.25° horizontal grid-spacing, and lateral boundaries were taken 3 hourly from the ECMWF operational forecasts. COSMO forecasts are evaluated using aircraft observations from the Saharan boundary layer in Section 3.

Version 2.4 of the Met Office large eddy model (LEM, Gray et al. 2001) was used to simulate the convection within the Saharan boundary layer for B301. Since in the region of interest the aircraft was at low level, no observed profiles were available, and the LEM was initialised with a profile from the COSMO simulation (12:00 UTC, 18° N 7.5° W). Small perturbations were added to the model to allow boundary-layer convection to develop, surface fluxes from the COSMO model were applied, and the mean wind profile was relaxed towards the profile from the COSMO model (to account for large scale forcings). A three-dimensional 20 km by 20 km by 20 km domain was used with horizontal grid-spacings of 200 m, and vertical grid-spacings of 50 m in the boundary layer. The standard run, which used the observed wind, was rerun using a 50 km by 50 km horizontal domain. This larger domain did not significantly affect the modelled boundary-layer convection. Gravity wave damping was applied above 13 km and the model uses a rigid base and lid and periodic lateral boundary conditions.

2.3 Cospectral analysis

The significance of the coherences between observed variables was determined as a function of spatial scale using spectral analysis (e.g. Matthews and Madden 2000 and Taylor et al. 2007). The coherency between two Fourier transforms can be described as a spectral version of the correlation function, and is based on the product of one spectrum with the complex conjugate of the other. In order to infer significance, it is necessary to smooth this product over a range of wavenumbers (the bandwidth); here a running mean has been employed. A larger bandwidth increases the spectral sampling but reduces the resolution at which wavenumber-dependent effects can be identified. The result is normalised by the smoothed amplitudes of the original spectra to deduce the coherency, which takes values between zero (not coherent) and one (coherent). Statistical significance can be inferred from the coherency by considering the expected coherency of white-noise signals as a simple function of bandwidth (Julian, 1975). The technique also allows the phase

[1]Estimated using data from GERBILS data from over the ocean using the Airborne Research Interferometer Evaluation System, which has previously been used to investigate the effect of mineral dust on thermal radiation in the atmospheric window region, (Highwood et al., 2003)

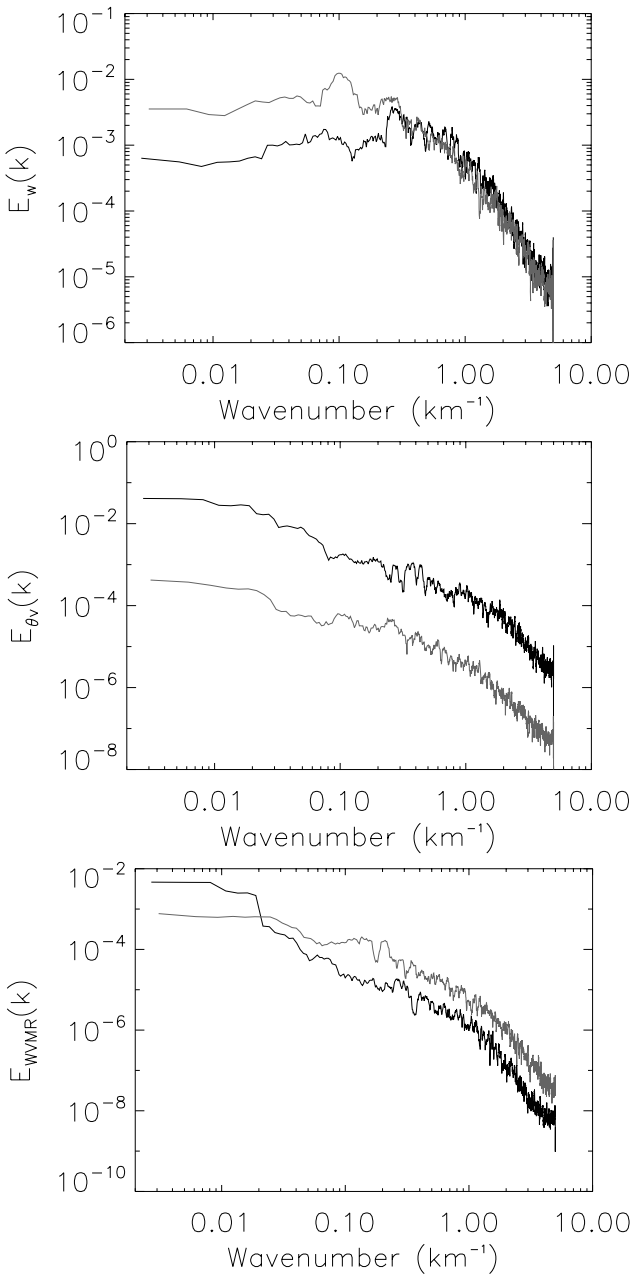

Fig. 2. Power spectra of vertical winds (w, top), virtual potential temperature (θ_v, middle) and water vapour mixing ratio (WVMR, bottom), from B302 (black line) and B301 (grey line).

difference for this coherency to be determined, as well as the "gain" i.e. the variation in one variable as a function of variations in another with which it is coherently related.

3 Results

Figure 2 shows the power spectra of vertical winds, virtual potential temperatures and WVMRs observed during B301 and B302.

For B302 the main peak in the power spectrum of vertical winds occurs on scale of approximately 4 km, which, as expected (Jonker et al., 1999), is of the order of the CBL depth ($\simeq$1.5 km, Sect. 3.1, Fig. 4). As a result, throughout this paper, "boundary-layer scale" is used to describe variations on scales 500 m and 5 km, *i.e.* on the order of the CBL depth. In this paper, "mesoscale" is used for any larger structures, (which are smaller than the synoptic scale).

For B302, variations in virtual potential temperature (θ_v) and WVMR are dominated by mesoscale contributions at scales around 100 km, particularly for WVMRs, but contributions from processes on the "boundary-layer scale" are still significant.

The vertical velocity spectrum for B301 is similar to that from B302, except that the peak occurs at a larger scale (approximately 10 km). The CBL depth during B301 was similar to B302 (1400 to 1800 m compared with 1200 to 1700 m, see Sects. 3.1 and 3.3) and so this shows a larger scale of organisation in the boundary-layer convection than for B302, for a similar CBL depth. As discussed in Sect. 3.3, this may be a result of the flight-path being oriented approximately along the axes of linearly organised boundary-layer convection (it is possible that rolls were also present during B302, but we would expect the more northerly boundary-layer wind to give a roll orientation more perpendicular to the aircraft flight track).

Variability in θ_v is lower for B301 than B302 and the boundary-layer scale contributions to variance in WVMR are much more significant for B301 (the peak at 10 km is also clear in the WVMR spectrum for B301). Surface latent heat fluxes in the Sahara are small compared with the surface sensible heat flux, and therefore boundary-layer convection is expected to create variability in WVMRs largely by the entrainment of dry air from the SRL into the CBL. The CBL was much moister during B301 compared with B302 (approximately 9.5 gkg^{-1} compared with 5 gkg^{-1}, Figs. 4 and 7) and COSMO simulations showed WVMRs in the SRL were similar on both days (approximately 4 gkg^{-1} and always drier than the CBL). Therefore, the greater boundary-layer scale contribution to variance in WVMR for B301 compared with B302 is probably because of the much stronger contrast between WVMRs in the CBL and SRL on this day. Furthermore, B301 was closer to the top of the CBL, where the effects of entrainment are likely to be more significant, but this is expected to increase the boundary-layer scale variability in both temperatures and WVMRs.

3.1 Flight B302, 28th June 2007

Figure 3a shows the low-level transect of B302 and surface albedo derived from MODIS satellite data (Gao et al., 2005; Houldcroft et al., 2008).

This shows that the flight crossed an area with a variety of albedo features, which is typical of the western Sahara. One particular albedo feature, at 8° W, stands out in the aircraft data (Fig. 4a, green line). This can be seen in the MODIS data (Fig. 3a) and was from a rocky valley and escarpment, with a minimum albedo of approximately 0.2, compared with the surrounding sandy desert with an albedo of 0.45 (Fig. 4a, green line). An increase in BT measured by the Heimann radiometer was also observed at 8° W (Fig. 4a, black line). This can be assumed to correspond to an increase in LST, which is consistent with the albedo anomaly. This high LST appears to have locally increased the potential temperature of the boundary layer at this location by approximately 2 K (Fig. 4a, b and c, red lines) and to be collocated with a region of convergence (Fig. 4c, blue line). Presumably, this anomaly in potential temperature is approximately in phase with the albedo anomaly as the albedo anomaly has an extent upstream, extending approximately in the wind direction (Fig. 3a and b).

This 2 K perturbation in boundary-layer potential temperature has the potential to significantly affect the vertical mixing of the SRL, since the SRL is weakly stratified (e.g. Figs. 1 and 5). In this case, where there is a change in orography collocated with the albedo feature, this effect may be enhanced by the effect of the orography on the boundary layer.

Other similar, but smaller, albedo features can also be seen in Fig. 4a, for example at 6.7, 7.8 and 9.2° W. For these features there is some evidence of convergence in the along track winds (Fig. 4c, blue line). The effects of these land surface variations on the boundary layer are investigated more quantitatively using spectral analysis (Sect. 3.2).

Dashed lines in Fig. 4 are from the COSMO forecast. This shows modelled potential temperatures within 2 K of those observed, WVMRs within 1 gkg^{-1} and along-track winds typically within 1 ms^{-1}. However, the windspeeds in COSMO were up to 6 ms^{-1} lower than observed, since the across-track northerly winds in COSMO were too weak. Northerly winds were stronger further north in COSMO, suggesting that the low-level convergence of the ITD may have been too far north in the model. Despite this, the location of the windspeed maximum, at around 8° W was well captured by the COSMO forecast.

The land surface in COSMO includes an albedo feature at 8° W. In the model, this feature has an albedo of approximately 0.18 compared with 0.2 elsewhere on the aircraft flight-track (Saharan albedos in COSMO are lower than observed from the aircraft or from MODIS, not shown). The atmosphere in COSMO responds to the change in land surface at 8° W, showing a weak local temperature maximum and WVMR minimum (Fig. 4). This supports the hypothe-

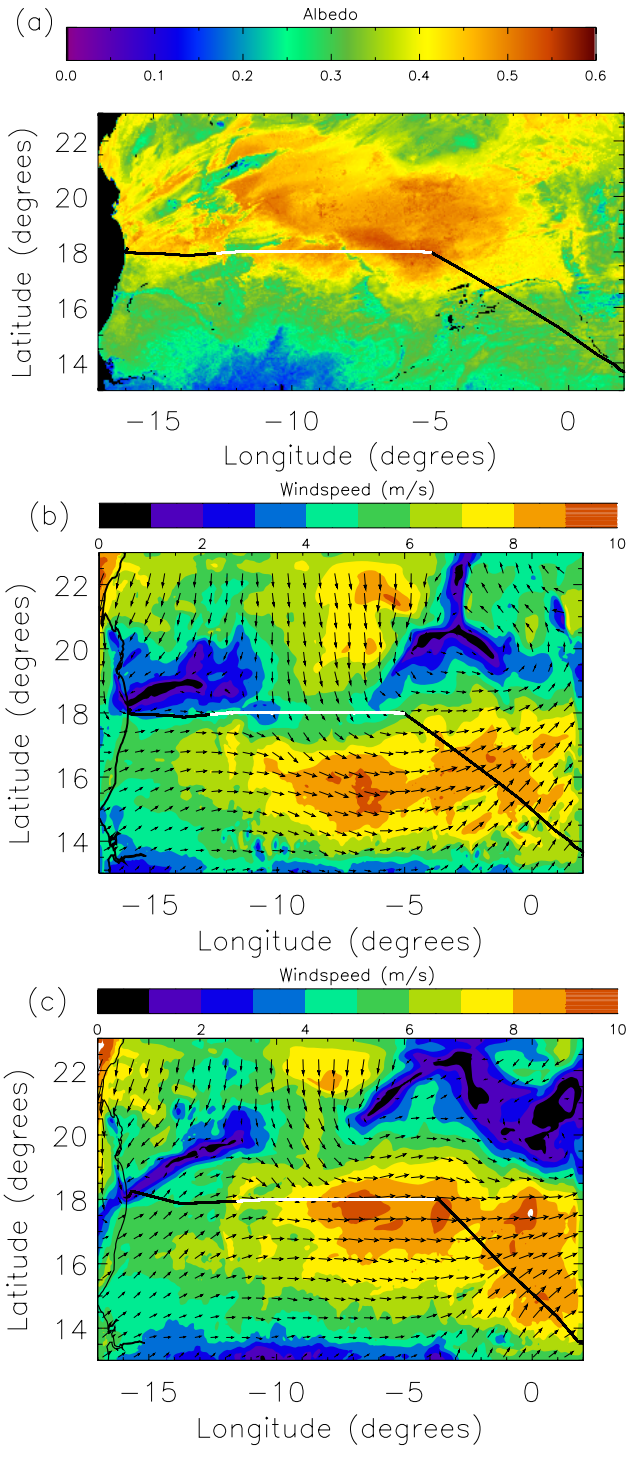

Fig. 3. Flight tracks of: **(a)** B302 (west to east) and albedo derived from MODIS satellite data, **(b)** B302 (west to east) and low-level winds from the COSMO simulation, **(c)** B301 (east to west) and low-level winds from the COSMO simulation. Flights were between Niamey (13.5° N and 2.1° E, not shown) and Nouakchott (18° N and 16° W). White lines show low-level legs.

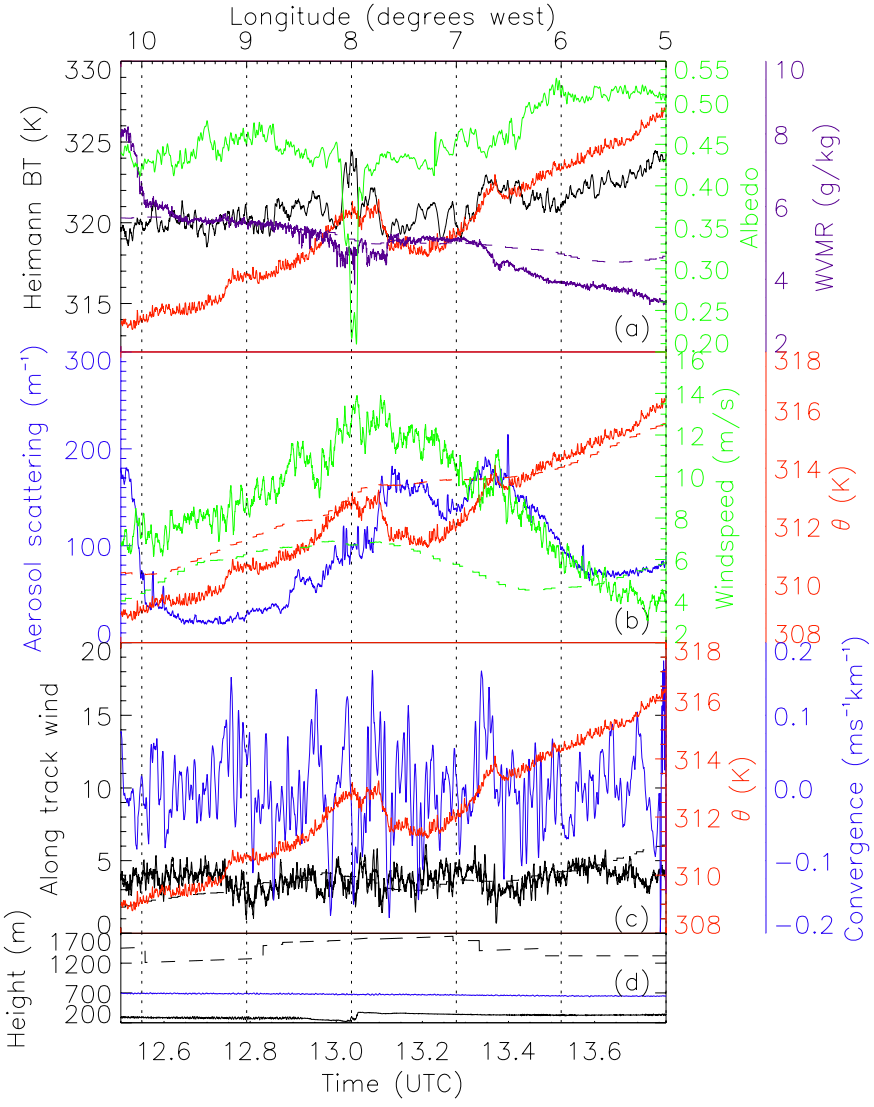

Fig. 4. Time smoothed data from the low-level transect of B302. "Albedo" was derived from observed upwelling and downwelling solar radiances. "Aerosol scattering" shows the aerosol scattering coefficient from the nephelometer in the blue channel. "Convergence" was calculated along the aircraft track. **(d)** shows the height of the orography (solid black line, derived from the aircraft GPS and radar altitudes), the aircraft GPS altitude (blue line) and the CBL depth from the COSMO model (dashed black line).

sis that the local temperature maximum observed at 8° W is indeed due to the change in land surface there.

Figure 5 shows the aircraft profile upwards from the eastern end of the low-level transect of B302 (the western profile was affected by the monsoon flow). Figure 5a shows that the boundary layer in COSMO was approximately 1 K too cold and 1 gkg^{-1} too moist, but the modelled boundary-layer depth was very close to that observed. Above the boundary layer, the SRL is observed to contain three main sub-layers (1500 to 2400 m, 2400 to 3300 m and 3300 to 5700 m). Of these, the lower two have similar dust and moisture contents, while the upper is drier and less dusty. Figure 5b again shows a more accurate representation of the westerly winds than the southerly winds in COSMO, although the trends with height are good and below 3 km values are typically within 3 ms^{-1} of the observations. The accuracy of the CBL depth shown by COSMO in Fig. 5a lends some support to its accuracy elsewhere along the low-level transect of B302. Figure 4d shows this modelled CBL depth (the dashed black line, and determined as the lowest model level where the potential temperature was not more than 0.5 K greater than the modelled mixed-layer depth). This shows that B302 was

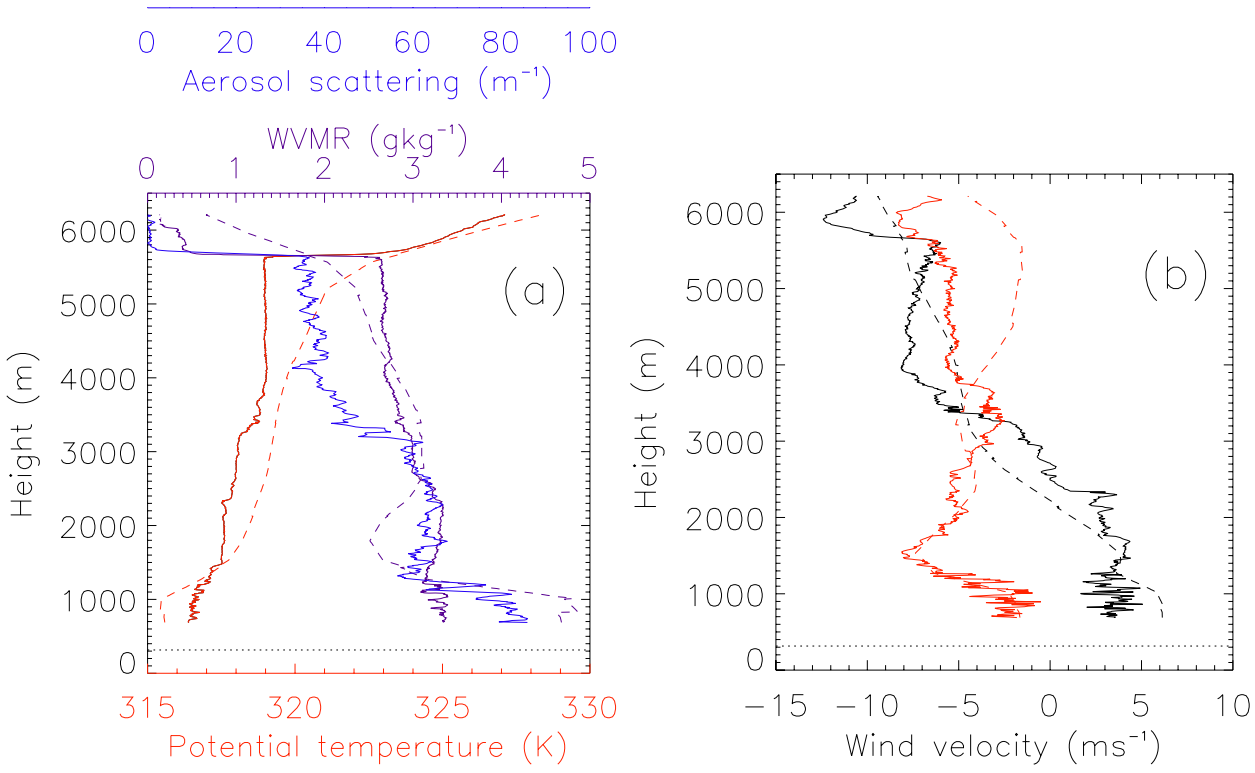

Fig. 5. Data from the aircraft profile upwards from the eastern end of the low-level leg of B302 (from 5.0° W 18.0° N to 3.9° W 17.4° N, 13.47 to 14:03 UTC). Observations are shown by solid lines and variables from the COSMO model are shown by dashed lines (interpolated in time and space to the point of observation). The horizontal dotted lines show the height of the ground at the start of the profile. **(a)** Shows potential temperature (red), WVMR (purple) and the aerosol scattering coefficient from the nephelometer in the blue channel (blue). **(b)** Shows westerly winds (black) and southerly winds (red).

within the lower part of the CBL (0.18 to 0.35 times the CBL depth), which is consistent with the observed convergence over warm land surface anomalies.

West of 9.5° W the air is moist and dusty (Fig. 4a and b, purple and blue lines). Simulations performed using the COSMO model showed this moist air remained from the previous day's monsoon flow (Fig. 3b and c), the monsoon air close to the ITD was usually observed to be dusty during GERBILS, as discussed by Marsham et al. 2008). Between 6° and 9° W the nephelometer data (Fig. 4b, blue line) show an area of increased dust loadings. The two main peaks in low-level dust loadings (at 6.8 and 7.5° W) are east of the position of the local maximum in windspeed (7.6 to 8° W). This is consistent with advection of dust into the flight-track from a location upstream, where the windspeed maximum was further to the east than the windspeed maximum on the flight-track. Such an eastwards displacement of the upstream windspeed maximum is shown by the COSMO model (Fig. 3b), although as noted there are significant errors in the COSMO wind field. Overall, this suggests that much of the dust observed was probably uplifted by the higher windspeeds upstream, rather than locally.

However, there appears to be some correlation between observed peaks in windspeed and observed peaks in dust loadings, for example at 8.5, 7.7 and 6.7° W (Fig. 4b). This suggests the possibility of some significant dust uplift occurring close to the flight track, which is again investigated using spectral analysis.

3.2 Cospectral analysis of data from flight B302

In order to investigate the effects of the land-atmosphere coupling in the Sahara, data from west of 9.5° W were rejected, since they were affected by the monsoon flow. For the remaining data cospectral analysis showed that there was a significant relationship between albedo and LST for all scales where a relationship between LST anomalies and boundary-layer properties were observed (i.e. >10 km, but in fact for all scales >2.5 km, not shown).

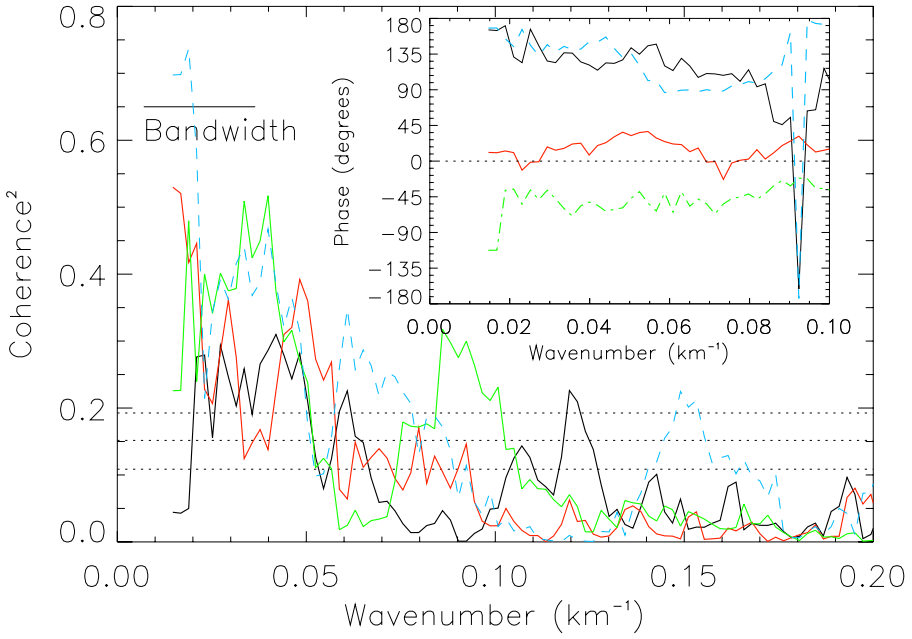

Fig. 6. The coherence and phase of relationships of Heimann BT (red line), along-track wind (black line), windspeed (green line), WVMR (pale blue dashed line) with θ_v for B302. Horizontal black dashed lines show 80, 90 and 95 % thresholds respectively (from bottom to top).

Figure 6 shows that at scales greater than approximately 10 km ($k<0.1$ km^{-1}) there is a significant relationship between LST and boundary-layer virtual potential temperature (θ_v), with the LST anomalies approximately 20 degrees out of phase with the θ_v, which is consistent with the along-track winds ($\simeq$4 ms^{-1}) resulting in the high buoyancy air being located downstream of the high LSTs and these LST anomalies having sufficient upstream extents to have observable effects on the boundary layer along the aircraft track. Effects on the CBL from LST anomalies with too small an upstream extent would have been impossible to observe, since they would have been advected downstream, away from the flight-track. Figure 6 also shows that there is a coherent relationship between along-track winds and θ_v at these scales, with convergence tending towards regions of high θ_v (a phase difference of 110° to 135° for $0.03<k<0.06$).

Analysis also showed a similar coherent relationship between along-track winds and LSTs at these scales (not shown). The derived gains showed LST anomalies affecting along-track winds by 0.25 to 0.5 ms^{-1}K^{-1} (not shown).

Figure 6 shows that on scales greater than 20 km the high θ_v regions tend to be drier (WVMR is out of phase with θ_v by between 135° and 180° on these scales). This may be from increased entrainment of dry air in such regions, or an increased Bowen ratio, or both. Windspeeds were also coherently related to θ_v on scales greater than 10 km, with their maximum downstream of the θ_v maximum (approximately –45° out of phase); across-track winds were greater than the along-track winds, so it is possible for the phase of the along-track winds and windspeed to be of opposite signs.

The analysis was then restricted to west of 6° W, restricting the track analysed to the data in the dust plume where local windspeeds were greater than 6 ms^{-1} and where local uplift is likely to be more significant. Figure 7 shows that for this region mesoscale variations in dust loadings depended on mesoscale variations in windspeed, for scales greater than 10 km ($k<0.1$ km^{-1}). If data from 5° to 6° W were included then this relationship was still significant, but less clear. Restricting the analysis to west of 6° W also showed that on scales of greater than 20 km regions of increased θ_v were also less dusty (not shown), possibly from entrainment of less dusty drier air in these regions, or from reduced dust uplift over darker rockier surfaces. It was not possible to unambiguously relate dust and LSTs, however; this is unsurprising given that the maximum dust uplift occurred upstream of the flight track, and the effects of land-surface itself on the potential for dust uplift.

3.3 Flight B301, 27th June 2007

B301 provided another long leg through the Saharan boundary layer, following a very similar path to B302 (Fig. 3), but monsoon air was present east of 6.6° W (and probably also convectively generated cold pools, as discussed by Marsham et al. 2008) and the monsoon flow again affected west of 9.5° W. As a result the profiles to and from the low-level leg were not of use in evaluating the representation of the Saharan CBL in COSMO. Marsham et al. (2008) show that for the profile at the eastern end of the low-level leg, which was affected by the monsoon, COSMO gave a good agreement with

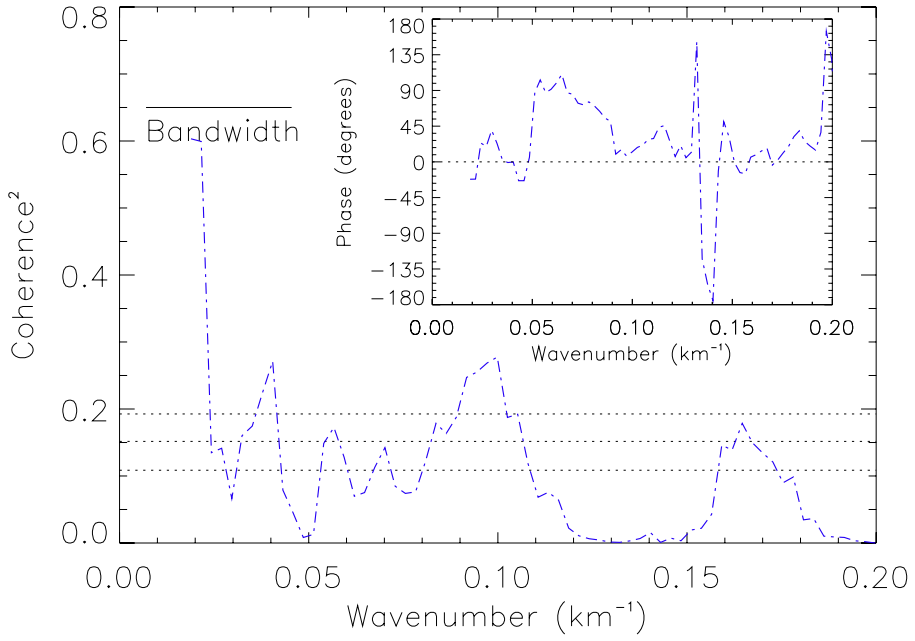

Fig. 7. As Fig. 6 but the relationship of dust (blue dash-dot line) with windspeed west of 6° W.

the broad features of this profile, but not the fine-structure of the layerings observed in the SAL. CBL depths from COSMO suggest that the low-level leg from B301 was at an altitude approximately in the middle of the CBL (Fig. 8d), which is expected to make identification of convergence or divergence over land-surface anomalies difficult.

Although boundary-layer windspeeds were similar during B301 and B302, along-track winds were greater during B301 than B302 (approximately 10 ms^{-1} compared with 4 ms^{-1}, Figs. 4 and 8c) and this is expected to decrease the effects of LST anomalies on boundary-layer temperatures and winds (Segal and Arritt, 1992). This is consistent with the observation that although for B301 there was some statistical significance to the coherence between LSTs, θ_v and along-track winds in the boundary layer (not shown) this effect was much less distinct than for B302. Links between albedos, LSTs and θ_v can still be observed in the low-level data from B301, however.

Figure 9 shows the details of the observations from 8.0° W. The low albedo escarpment (at 8.0° W) again led to an increased Heimann BT. A region of high buoyancy (θ_v, red line) is observed downstream of this LST anomaly. This is further downstream than shown for B302 due to the larger along-track winds (Figs. 4 and 9c). This corresponds to a region of divergence in along-track winds (Fig. 9c), which suggests at this point the aircraft was towards the upper half of the CBL and that the boundary-layer depth from COSMO was too large. The magnitude of the perturbation to the boundary-layer potential temperature ($\simeq$0.5 K) again has the potential to significantly affect the vertical mixing of the weakly stratified SRL (Fig. 1), but is smaller than observed during B302 (as expected from the greater along-track winds on this day). The COSMO forecast shows no clear effect from the low albedo escarpment at 8.0° W, but, as already noted, the change of albedo in COSMO is smaller than observed.

Decreased BTs from high albedo features can be seen at 8.7 and 7.0° W (Fig. 8a) which perhaps lead to decreased θ_v. The narrower high albedo at 9.2° W is associated with a small decrease in BT, and any effect on θ_v is unclear. The elevated θ_v between 7.2 and 7.6° W does not appear to be related to any LST anomaly.

Figure 8b shows windspeeds (which are dominated by the along-track winds) increasing from west to east, which is consistent with the COSMO simulation (dashed lines in Fig. 8 and also see Fig. 3c). COSMO gives an accurate forecast for the low-level leg, with temperatures within 1 K of those observed, WVMRs approximately 2 gkg^{-1} too moist and east of 8.3° W, windspeeds within 1 ms^{-1} of those observed (Fig. 8). The errors in windspeed increase towards the west, reaching approximately 4 ms^{-1} at 9.5° W (Fig. 8).

Dust loadings west of 8.8° W were low, but are observed to increase towards the east with the increasing windspeeds (Fig. 8b). Winds were oriented from approximately 260° i.e. almost along the west to east flight track. Windspeeds upstream were lower than those at the point of observation and COSMO simulations showed 10 m windspeeds increasing from midnight to the time of observation. East of 8.5° W there was a strong positive correlation between observed windspeeds and aerosol scattering (Pearson

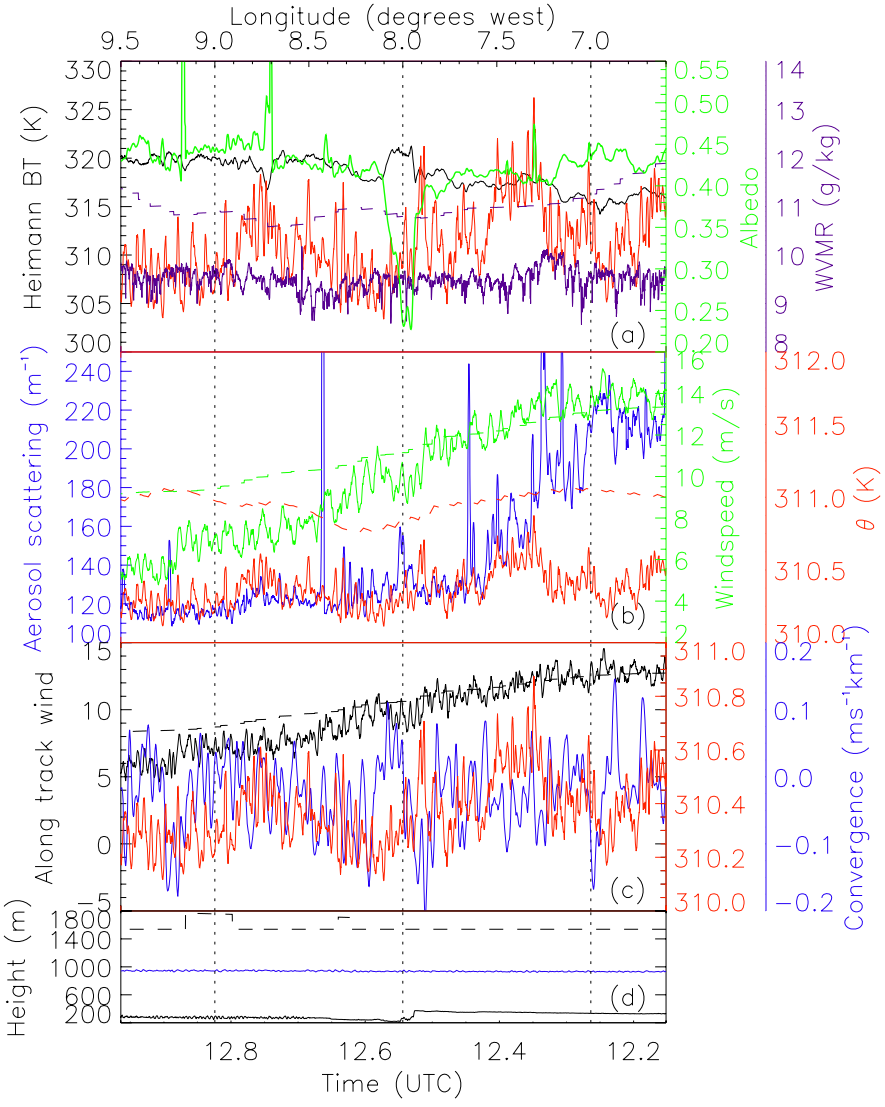

Fig. 8. As Fig. 4, but for B301, for the portion of the low level flight unaffected by convectively generated cold pools or the monsoon flow.

correlation coefficient=0.8, not shown). Therefore, it is likely that the dust observed was uplifted locally along the flight-track, in the area of higher windspeeds shown by COSMO to be oriented along the flight track (Fig. 3c, 6.6 to 8.5° W). Cospectral analysis of data from B301 is not shown, but at scales between 5.5 to 12.5 km, which includes the 10 km scale peak in the power spectrum of vertical winds observed for B301, it showed a significant (90%) coherent relationship between nephelometer scattering data, WVMRs and vertical winds. Both WVMRs and the scattering were in phase with the vertical winds showing moist dusty updraughts and cleaner drier downdraughts on these scales. This is consistent with dust uplift occurring at the surface and the entrainment of cleaner air into the CBL from the SRL above.

3.3.1 The contribution to dust uplift from boundary-layer convection evaluated using LEM simulations

A region of high winds leading to local dust uplift has been identified from flight B301 (approximately 6.6 to 8.5° W, Sect. 3.3). In this section, an LEM simulation is used to investigate the expected contribution to dust uplift made by the boundary-layer circulations resolved by the LEM, that would not be resolved by a regional or global model. The LEM (described in Sect. 2) was initialised using a COSMO profile from 7.5° W (aircraft profiles were affected by the monsoon flow).

Figure 10a shows linearly organised boundary-layer convection ("rolls") in the LEM oriented approximately east-west. The roll-spacing of approximately 2.5 km is well

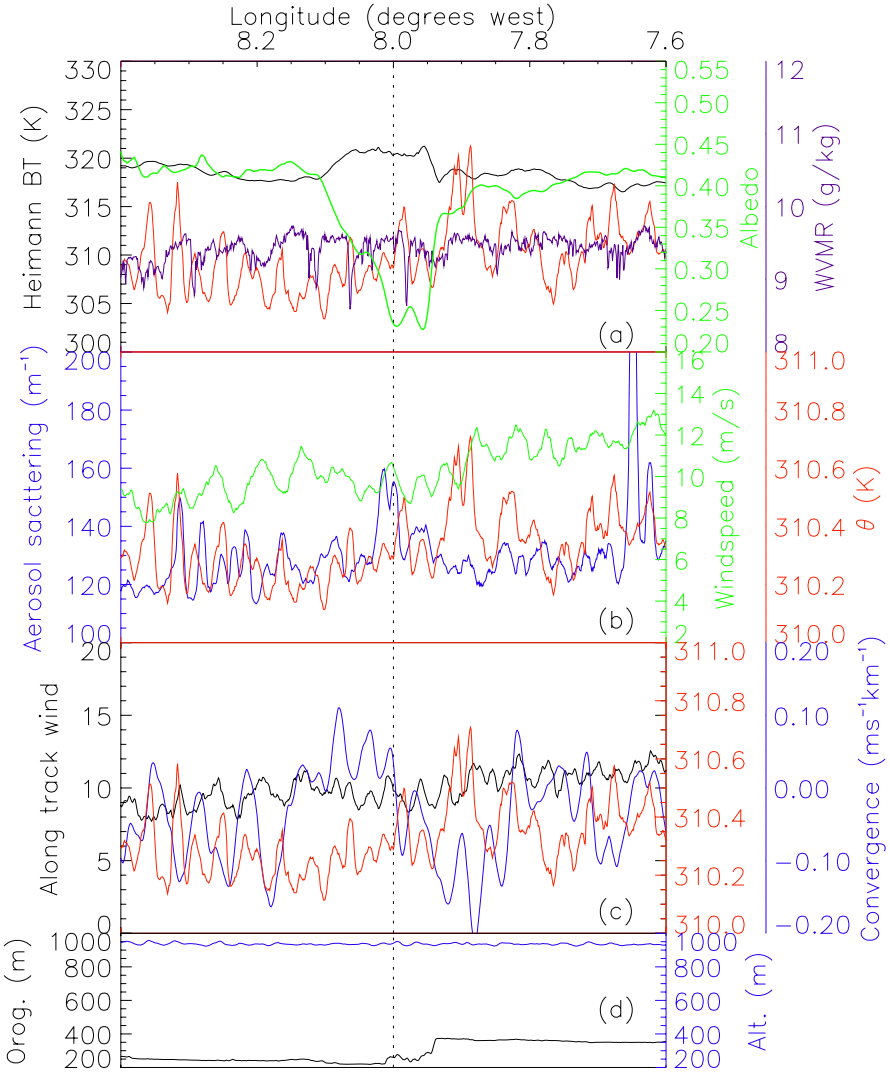

Fig. 9. As Fig. 8 but showing details of the effects of the rocky escarpment at 8.0° W on the boundary-layer (the CBL depth from COSMO is not shown in (d) in order to show the details of the orography).

resolved by the LEM grid-spacing of 200 m. The rolls are relatively disorganised, but they became more linear if the horizontal mean of the LEM potential temperature profile was relaxed towards that of the COSMO model (their alignment was unchanged, not shown). Power spectra of vertical velocities from west-east transects through the LEM modelled fields showed peaks at approximately 4 and 10 km, and a gap at approximately 7 km (clearest for the simulation using the 50 km domain). This is consistent with the hypothesis that the linear organisation of boundary-layer convection was responsible for the peak in the power spectrum of vertical winds from flight B301 at a scale of approximately 10 km (Fig. 2a).

The probability density function of the windspeeds from the LEM (calculated from the two-dimensional field of winds at the aircraft height in the LEM) is very similar to that observed (Fig. 10b), with a standard deviation of 0.97 ms^{-1} for LEM and 0.87 ms^{-1} for the observations. This supports the use of the LEM for investigating the role of boundary-layer circulations in dust uplift in this case, although the LEM will fail to capture details of features with scales of less than approximately 1 km (five times the grid-spacing). At 13:00 UTC the windspeeds at the lowest level in the LEM (33 m a.g.l.) varied from 5.4 to 15.8 ms^{-1}, with a mean of 9.9 ms^{-1}. These variations in low-level winds contribute to the non-linear process of dust uplift.

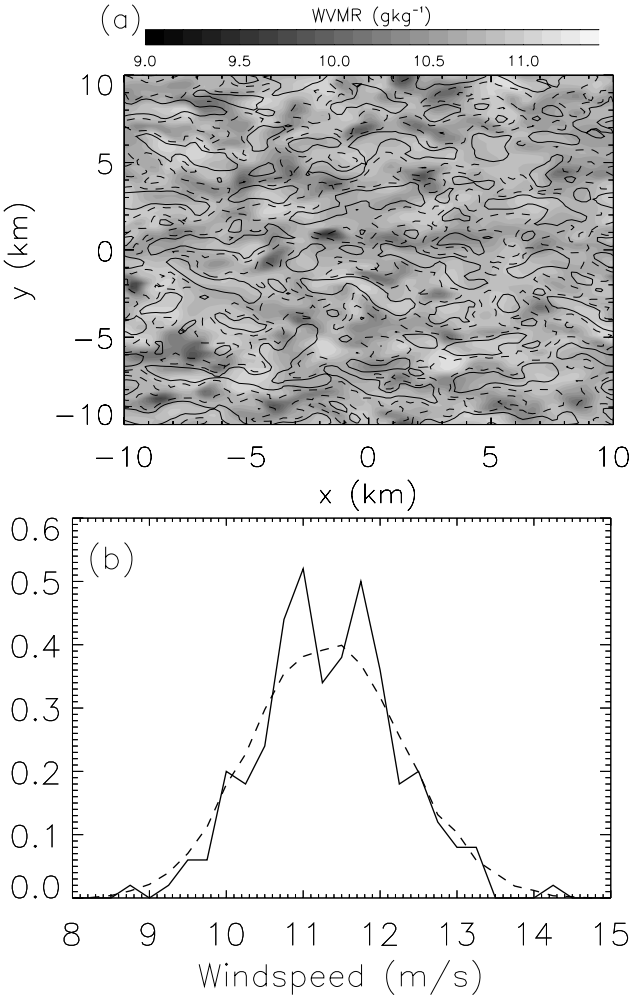

Fig. 10. Results from LEM simulations of the B301 boundary layer at 13:00 UTC from 627 m above the ground: **(a)** WVMR (greyscaled) and vertical velocities (line contours at ± 1 ms^{-1}, dashed are negative). **(b)** Probability density functions of windspeed from the LEM (dashed line), and observations from 7.65±0.1° W (solid line,).

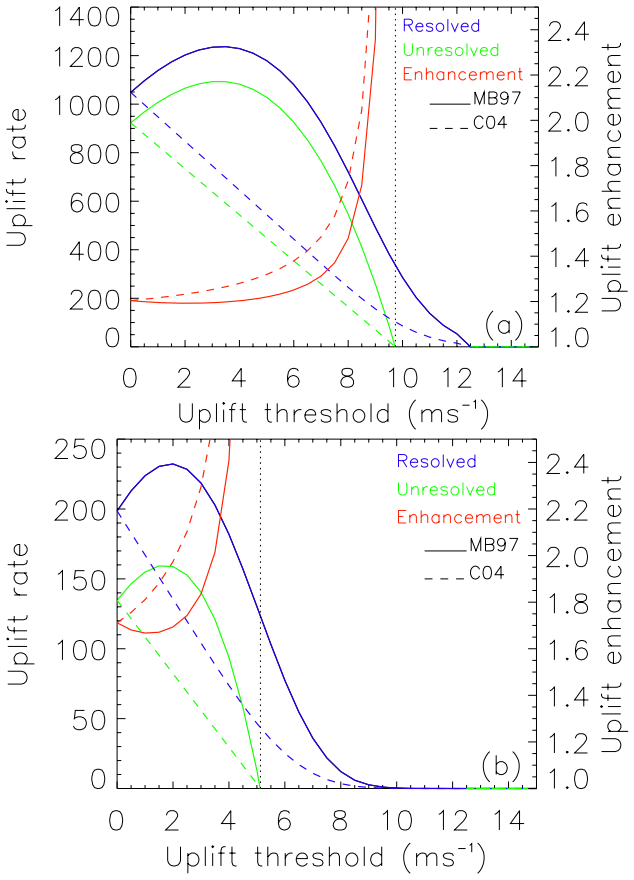

Fig. 11. Dust "uplift rates" (actually windspeeds cubed) from equations 1 ("MB97", thick lines) and 2 ("C04", dashed lines) using the LEM winds (blue lines, "resolved" winds) and the mean wind in the LEM (green lines, "unresolved" wind). "Enhancement" factors i.e. the fractional increases in uplift from using the "resolved" winds are also shown (red lines). **(a)** Results from the standard LEM run. **(b)** Results from an LEM run with the mean wind in the model reduced by a factor of two.

Dust uplift (F) can be parametrised as a function of friction velocity (u_*) cubed with a threshold friction velocity (u_{*T}). Marticorena and Bergametti (1997) Eq. 5 gives,

$$F \propto u_*^3(1+R)(1-R^2), \quad (1)$$

where $R{=}u_{*T}/u_*$. u_{*T} depends on the particle size and Marticorena and Bergametti (1997) integrate over the size distribution, with contributions from different sizes weighted by their areal abundance. Cakmur et al. (2004) uses the simpler formula,

$$F \propto u_*^2(u_* - u_{*T}), \quad (2)$$

for $u_* \geq u_{*T}$. In the LEM, for a convective boundary layer,

$$u_* = k.u_1/(log(z/z_0) - \psi)), \quad (3)$$

where u_1 is the wind velocity at the lowest model level (z_1), z_0 is the roughness length of the surface, k is the von Kármán constant, and ψ accounts for the stability (Gray et al., 2001). Therefore, for a constant surface roughness, if effects from any spatial variations in the stability are neglected (as used by Cakmur et al. 2004) u_* is proportional to u_1. A calculation of the variability in u_*, with and without spatial variations in ψ, showed that the variability in u_* was completely dominated by variations in u_1 (not shown), justifying the neglect of the spatial variability in ψ.

We can therefore obtain an estimate of the effects of the modelled boundary-layer convection on dust uplift by comparing the rates calculated using the LEM winds from the lowest model level, and rates calculated from the windspeed derived from the mean wind velocities in the lowest model

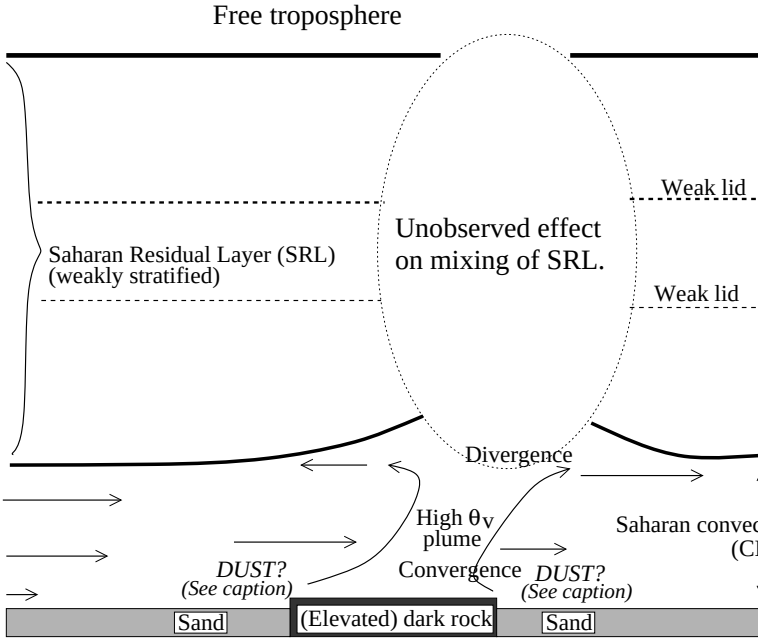

Fig. 12. Schematic of the effects of an albedo anomaly on the Saharan boundary layer. Note that observations show statistically significant links between: (i) mesoscale variations in LSTs, θ_v and winds and (ii) windspeeds and dust, but do not show significant links between LSTs and dust.

level (using Eqs. 1 and 2). We do not consider the effects of particle size on the uplift threshold, but look at uplift rates as a function of this threshold.

Cakmur et al. (2004) suggest that 10 m windspeed thresholds for dust uplift in the Sahara are typically 8 to 10 ms^{-1}. For B301, Fig. 11a shows that the boundary-layer convection resolved by the LEM increases dust uplift by approximately 14% for a zero threshold and this increases as the threshold increases, with the details depending on whether the uplift parametrisation of Marticorena and Bergametti (1997) or Cakmur et al. (2004) is used. An uplift threshold of 8 ms^{-1} (Cakmur et al., 2004) results in an enhancement of 30%. The enhancement of uplift is greatest when the mean wind is just less than the threshold and the rolls give significant uplift that would not otherwise occur. If the mean horizontal winds in the LEM are decreased by a factor of two, the uplift enhancement is increased, with a minimum enhancement of 70% (Fig. 11b). This occurs since the windspeed variations from boundary-layer convection become more significant as the speed of the mean boundary-layer wind is decreased (note that at this lower windspeed the convection in the LEM was more cellular than linear). However, at low windspeeds processes such as dust devils, which would not be resolved by the LEM setup used, are expected to dominate (Koch and Renno, 2005). These effects of boundary-layer circulations on dust uplift are not included in any global model where modelled dust uplift is a function of u_*, and u_* depends on the resolved wind so that u_* tends to zero as the resolved wind tends to zero.

It is not clear to what extent parametrisations and thresholds used by Cakmur et al. (2004) and Marticorena and Bergametti (1997) are applicable on the small spatial and temporal scales resolved by the LEM. Therefore the quantitative details of the enhancement discussed above remain somewhat uncertain. In addition, scales smaller than those by the LEM may be significant for dust uplift (Koch and Renno, 2005). However, despite these uncertainties, the estimated enhancement of uplift, support the other existing evidence that boundary-layer convection plays a significant role in driving dust uplift in the Sahara (Cakmur et al., 2004).

4 Conclusions

Results from low level flights made during the GERBILS field campaign have been used to demonstrate the effects of mesoscale land surface temperature (LST) anomalies (which were related to albedo anomalies) on the virtual potential temperatures and winds in the boundary layer and mesoscale wind variations on dust loadings. LEM simulations, based on the GERBILS observations, have been used to investigate the enhancement of dust uplift by boundary-layer convection. These boundary-layer and mesoscale processes are

unrepresented in many climate models, but are expected to have significant impacts on the uplift and vertical transport of desert dust. Mesoscale effects in particular are difficult to parametrise in such models (for example, Zheng and Pielke 1995).

Figure 12 shows a schematic of the mesoscale processes observed. On a day with high windspeeds ($\simeq$10 ms^{-1}), but relatively weak along-track winds ($\simeq$4 ms^{-1}), land surface albedo and temperature anomalies of scales greater than 10 km generated significant perturbations in buoyancy in the CBL (up to approximately 2 K). These anomalies were shown to lead to convergence in the boundary-layer winds on these scales, and are expected to affect vertical mixing of the SRL, and so dust transport. This is consistent with the observations of decreased WVMRs, corresponding to increased θ_v on these scales, which may be from increased entrainment drying of the boundary layer, or an increased Bowen ratio of the land surface.

Mesoscale (greater than 10 km) variations in boundary-layer dust loadings were also shown to depend on variations in windspeed on these scales. This was most significant where observed windspeeds exceeded 6 ms^{-1}, which presumably allowed dust uplift to occur locally.

On a day with greater along-track windspeeds ($\simeq$ 10ms^{-1}) the effects of LST anomalies were, as expected, not as significant, but were still observed. A region of the flight-track where dust was occurring locally was identified from this day, and LEM simulations based on this case showed linearly organised boundary-layer convection. This organisation may explain the observation that the power spectrum of vertical winds on this day had its peak at approximately 10 km, a larger scale than observed on the next day (B302), and significantly larger than the modelled CBL depth from COSMO ($\simeq$1.5 km). There was also a significant coherence between vertical winds and both aerosol scattering and WVMRs on this scale (scales between 5.5 to 12 km), showing moist dusty updraughts. This is consistent with dust uplift at the surface and the entrainment of cleaner drier air from above.

Within the region of observed dust uplift, assuming an uplift threshold of 8 ms^{-1}, the LEM results showed that the boundary-layer convection resolved by the LEM is expected to have increased dust uplift by approximately 30%, compared with uplift calculated using the mean wind.

The enhancement of uplift by boundary-layer convection is larger for lower boundary-layer windspeeds, and most significant when the mean wind is below the threshold for dust uplift and the convection leads to uplift that would not otherwise occur. Any possible dependence of the uplift enhancement on the form of the boundary-layer convection (rolls, cells etc) was beyond the scope of this study. The applicabilities of dust uplift parametrisations and thresholds in the literature to small spatial and temporal scales are not clear, which increases the uncertainty in the details of these enhancement effects. We recommend that the range of the applicability of such parametrisations should be investigated.

Dust loadings in the SRL have important effects on climate. For dust to get into the SRL it must be uplifted from the surface and then transported vertically out of the CBL. The SRL is only weakly stratified, however, so even small ($\simeq$1 K) perturbations to CBL temperatures may significantly affect the vertical mixing (Fig. 12). These observations show that such variations can be induced by land surface anomalies, but any effects within the SRL could not be evaluated due to an absence of suitable data from between 1 km and the top of the SRL. In addition, no observations were available from days with light winds, when we expect the effects of the mesoscale (Segal and Arritt, 1992) and boundary-layer circulations to be increased. We therefore suggest that the impacts of these processes on dust uplift and transport are investigated using numerical modelling, or using future observational datasets.

Acknowledgements. This project was funded by the Natural Environment Research Council (NERC: NER/O/S/2002/00971) and AMMA-EU/UK. We would like to thank Jim Haywood (Met Office, UK) for organising the GERBILS field campaign; the staff of FAAM, whose hard work allowed the GERBILS field campaign to run so smoothly; the UK Met Office, for access to dust forecasts from their Crisis Area Model (CAM) and for providing access to the ECMWF data; Dr Conny Schwierz (University of Leeds, UK) for facilitating access to this ECMWF data, Sarah Jones (Universität Karlsruhe and Forschungszentrum Karlsruhe, Germany) for enabling use of the COSMO model, and Chris Taylor (Centre for Ecology and Hydrology, UK) for facilitating access to Saharan albedo data. Finally we would like to thank Marie Lothon whose detailed review allowed significant improvements to be made to the paper.

Edited by: R. MacKenzie

References

Cakmur, R. V., Miller, R. L., and Torres, O.: Incorporating the effect of small-scale circulations upon dust emission in an atmospheric general circulation model, J. Geophys. Res.-Atmos., 109, D07201, doi:10.1029/2003JD004067, 2004.

Cakmur, R. V., Miller, R. L., Perlwitz, J., Geogdzhayev, I. V., Ginoux, P., Koch, D., Kohfeld, K. E., Tegen, I., and Zender, C. S.: Constraining the magnitude of the global dust cycle by minimizing the difference between a model and observations, J. Geophys. Res.-Atmos., 111, D06207, doi:10.1029/2005JD005791, 2006.

Chaboureau, J. P., Tulet, P., and Mari, C.: Diurnal cycle of dust and cirrus over West Africa as seen from Meteosat Second Generation satellite and a regional forecast model, Geophys. Res. Lett., 34, L02822, doi:10.1029/2006GL024441, 2007.

Doms, G. and Schättler, U.: A description of the nonhydrostatic Regional Model LM. Part I: Dynamics and Numerics, Consortium for Small-Scale Modelling (COSMO), download at: http://www.cosmo-model.org, 2002.

Field, P. R., Möhler, O., Connolly, P., Krämer, M., Cotton, R., Heymsfield, A. J., Saathoff, H., and Schnaiter, M.: Some ice nucleation characteristics of Asian and Saharan desert dust, At-

mos. Chem. Phys., 6, 2991–3006, 2006, http://www.atmos-chem-phys.net/6/2991/2006/.

Gammo, M.: Thickness of the dry convection and large-scale subsidence above deserts, Bound.-Lay. Meteorol., 79, 265–278, 1996.

Gao, F. C., Schaaf, A., Strahler, A., Roesch, A., Lucht, W., and Dickinson, R.: MODIS bidirectional reflectance distribution function and albedo Climate Modeling Grid products and variability of albedo for major global vegetation types, J. Geophys. Res., 110, D01104, doi:10.1029/2004JD005190, 2005.

Gray, M. E. B., Petch, J., Derbyshire, S. H., Brown, A. R., Lock, A. P., and Swann, H. A.: Version 2.3 of the Met. Office large eddy model, The Met. Office, Exeter, UK, 2001.

Haywood, J. M., Allan, R., Culverwell, I., Slingo, T., Milton, S., Edwards, J., and Clerbaux, N.: Can desert dust explain the outgoing longwave radiation anomaly over the Sahara during July 2003?, J. Geophys. Res.-Atmos., 110, D05105, doi:10.1029/2004JD005232, 2005.

Highwood, E. J., Haywood, J. M., Silverstone, M. D., Newman, S. M., and Taylor, J. P.: Radiative properties and direct effect of Saharan dust measured by the C-130 aircraft during SHADE. 2: Terrestrial spectrum, J. Geophys. Res.-Atmos., 108(D18), 8578, doi:10.1029/2002JD002552, 2003.

Houldcroft, C., Grey, W., Barnsley, M., Taylor, C., Los, S., and North, P.: New vegetation albedo parameters and global fields of background albedo derived from MODIS for use in a climate model, J. Hydrometeorol., doi:10.1175/2008JHM1021.1, in press, 2008.

Jones, C., Mahowald, N., and Luo, C.: Observational evidence of African desert dust intensification of easterly waves, Geophys. Res. Lett., 31, L17208, doi:10.1029/2004GL020107, 2004.

Jonker, H. J. J., Duynkerke, P. G., and Cuijpers, J. W. M.: Mesoscale fluctuations in scalars generated by boundary layer convection, J. Atmos. Sci., 56, 801–808, 1999.

Julian, P. R.: Comments on the determination of significance levels of the coherency statistic, J. Atmos. Sci., 32, 836–837, 1975.

Koch, J. and Renno, N. O.: The role of convective plumes and vortices on the global aerosol budget, Geophys. Res. Lett., 32, L18806, doi:10.1029/2005GL023420, 2005.

Mahowald, N. M., Baker, A. R., Bergametti, G., Brooks, N., Duce, R. A., Jickells, T. D., Kubilay, N., Prospero, J. M., and Tegen, I.: Atmospheric global dust cycle and iron inputs to the ocean, Global Biogeochem. Cy., 19, GB4025, doi:10.1029/2004GB002402, 2005.

Mahowald, N. M., Muhs, D. R., Levis, S., Rasch, P. J., Yoshioka, M., Zender, C. S., and Luo, C.: Change in atmospheric mineral aerosols in response to climate: Last glacial period, preindustrial, modern, and doubled carbon dioxide climates, J. Geophys. Res.-Atmos., 111, D10202, doi:10.1029/2005JD006653, 2006.

Marsham, J. H., Parker, D. J., Grams, C. M., Taylor, C. M., and Haywood, J. M.: Uplift of Saharan dust south of the intertropical discontinuity, J. Geophys. Res.-Atmos., 113, D21102, doi:10.1029/2008JD009844, 2008.

Marticorena, B. and Bergametti, G.: Modelling of the atmospheric dust cycle 2. Simulation of Saharan dust sources, J. Geophys. Res.-Atmos., 102, 4387–4404, 1997.

Matthews, A. J. and Madden, R. A.: Observed propogation and structure of the 33-h atmopsheric Kelvin wave, J. Atmos. Sci., 57, 3488–3497, 2000.

Parker, D. J., Thorncroft, C. D., Buron, R. R., and Diongue-Niang, A.: Analysis of the African easterly jet, using aircraft observations from the JET2000 experiment, Quart. J. Roy. Meteor. Soc., 131, 1461–1482, 2005.

Pérez, C., Nickovic, S., Pejanovic, G., Baldasano, J. M., and Ozsoy, E.: Interactive dust-radiation modeling: A step to improve weather forecasts, J. Geophys. Res.-Atmos., 111, D10202, doi:10.1029/2005JD006579, 2006.

Segal, M. and Arritt, R. W.: Nonclassical mesoscale circulations caused by surface sensible heat-flux gradients, B. Am. Metor. Soc., 73, 1593–1604, 1992.

Stephens, G. L., Wood, N. B., and Pakula, L. A.: On the radiative effects of dust on tropical convection, Geophys. Res. Lett., 31, L23112, doi:10.1029/2004GL021342, 2004.

Takemi, T., Yasui, M., Zhou, J. X., and Liu, L. C.: Role of boundary layer and cumulus convection on dust emission and transport over a midlatitude desert area, J. Geophys. Res.-Atmos., 111, D11203, doi:10.1029/2005JD006666, 2006.

Tanaka, T. Y. and Chiba, M.: A numerical study of the contributions of dust source regions to the global dust budget, Global Planet. Change, 52, 88–104, 2006.

Taylor, C. M., Parker, D. J., and Harris, P. P.: An observational case study of mesoscale atmospheric circulations induced by soil moisture, Geophys. Res. Lett., 34, L15801, doi:10.1029/2007GL030572, 2007.

Tompkins, A. M., Cardinali, C., Morcrette, J. J., and Rodwell, M.: Influence of aerosol climatology on forecasts of the African Easterly Jet, Geophys. Res. Lett., 32, L10801, doi:10.1029/2004GL022189, 2005.

Washington, R., Todd, M. C., Engelstaedter, S., Mbainayel, S., and Mitchell, F.: Dust and the low-level circulation over the Bodele Depression, Chad: Observations from BoDEx 2005, J. Geophys. Res.-Atmos., 111, D03201, doi:10.1029/2005JD006502, 2006.

Woodward, S.: Modeling the atmospheric life cycle and radiative impact of mineral dust in the Hadley Centre climate model, J. Geophys. Res.-Atmos., 106, 18 155–18 166, 2001.

Zakey, A. S., Solmon, F., and Giorgi, F.: Implementation and testing of a desert dust module in a regional climate model, Atmos. Chem. Phys., 6, 4687–4704, 2006, http://www.atmos-chem-phys.net/6/4687/2006/.

Zheng, X. and Pielke, R. A.: Landscape-Induced Atmospheric Flow and its Parameterization in Large-Scale Numerical Models, J. Climate, 8, 1156–1177, 1995.